Geophysical Research Letters

Key Points:
- The trough minimum location moves quickly equatorward and poleward during the storm main and recovery phases, respectively
- The longitudinal distribution of the trough minimum location shows a significant variation with a scale of 1,000–2,500 km
- The trough minimum location is located near the footprint of the plasmapause signature in the inner magnetosphere

Temporal and Spatial Variations of Storm Time Midlatitude Ionospheric Trough Based on Global GNSS-TEC and Arase Satellite Observations

Atsuki Shinbori[1] (iD)**, Yuichi Otsuka[1]** (iD)**, Takuya Tsugawa[2], Michi Nishioka[2]** (iD)**, Atsushi Kumamoto[3]** (iD)**, Fuminori Tsuchiya[4]** (iD)**, Shoya Matsuda[5], Yoshiya Kasahara[6]** (iD)**, Ayako Matsuoka[5]** (iD)**, J. Michael Ruohoniemi[7]** (iD)**, Simon G. Shepherd[8], and Nozomu Nishitani[1]** (iD)

[1]Institute for Space-Earth Environmental Research, Nagoya University, Nagoya, Japan, [2]National Institute of Information and Communications Technology, Tokyo, Japan, [3]Department of Geophysics, Tohoku University, Sendai, Japan, [4]Planetary Plasma and Atmospheric Research Center, Tohoku University, Sendai, Japan, [5]Japan Aerospace Exploration Agency, Institute of Space and Astronautical Science, Sagamihara, Japan, [6]Graduate School of Natural Science and Technology, Kanazawa University, Kanazawa, Japan, [7]Center for Space Science and Engineering Research, Virginia Tech, Blacksburg, VA, USA, [8]Thayer School of Engineering, Dartmouth College, Hanover, NH, USA

Abstract Temporal and spatial variations of the midlatitude ionospheric trough during a geomagnetic storm on 4 April 2017 have been investigated using Global Navigation Satellite System total electron content data together with Arase satellite observations. After the geomagnetic storm commencement, the trough minimum location moves equatorward from 60 to 48° in geomagnetic latitude within 4 hr. The trough minimum location identified from the Global Navigation Satellite System total electron content data is located near the footprint of an abrupt drop of electron density detected by the Arase High-Frequency Analyzer instrument. The longitudinal variation of the trough minimum location shows a significant variation with a scale of 1,000–2,500 km during both storm and quiet times. This phenomenon has not yet been reported by previous studies. After the onset of the storm recovery phase, the trough minimum location rapidly moves poleward back to the quiet time location within 4 hr.

Plain Language Summary Geomagnetic storms lead to a sever change in the plasma environment in the ionosphere and magnetosphere. Because their storm time disturbances in these regions cause an enhancement of positioning error and satellite anomaly due to the ionospheric electron density variation and magnetospheric high-energy particles, to clarify the characteristics of storm time variation of plasma environment and its physical mechanism is essential for prediction of the Geospace environmental change as space weather. In this study, we analyzed global positioning system total electron content data and Arase satellite observations in the inner magnetosphere to monitor a storm time change in the shape of the plasmasphere that controls the generation and propagation of plasma waves. Our analysis results show that the location of the midlatitude trough minimum identified from the total electron content data rapidly moves equatorward and poleward within 4 hr during the main and recovery phases. The location of the midlatitude trough minimum almost corresponds to that of the plasmapause detected by the Arase satellite. The longitudinal distribution of the midlatitude trough minimum shows a significant variation with its scale of 1,000–2,500 km. This feature is also seen during a geomagnetically quiet time. This phenomenon has not yet been reported by previous works.

1. Introduction

A geomagnetic storm is characterized by a significant decrease of the middle- and low-latitude *H* component of the geomagnetic field due to the development of ring current in the inner magnetosphere. The development is caused by the injection of plasmasheet particles into the inner magnetosphere associated with an enhanced convection electric field in the magnetosphere via a reconnection process between the southward interplanetary magnetic field (IMF) and Earth's magnetic field (e.g., Tsurutani et al., 2006). The enhanced convection electric field leads to a dramatic effect on the dynamics of the ionosphere and plasmasphere such as the formation of a plasmaspheric plume (e.g., Goldstein & Sandel, 2005; Moldwin et al., 2004; Yizengaw et al., 2008) and its ionospheric signature (e.g., Foster et al., 2002, 2004; Foster & Rideout, 2005; Yizengaw et al.,

2006, 2008). The convection electric field produces a plasma density enhancement in the ionosphere with a narrow structure which is named storm-enhanced density (SED; Foster, 1993).

Recent studies have revealed that SED structure in the ionosphere is linked to the erosion of the plasmasphere and the formation of a sharp plasmapause due to the strong subauroral polarization stream (SAPS; Foster & Vo, 2002), and coincides with the plasmaspheric plume and plasmapause (e.g., Yizengaw et al., 2005, 2006). The SAPS electric field is directed poleward and is formed in a closure current region between the region 1 and region 2 field-aligned currents. The intense electric field enhances the recombination process in the F region of the ionosphere due to increased ion-neutral frictional heating and ion temperature (Schunk et al., 1976). As a result, the midlatitude trough is formed with a sharp density gradient equatorward of the trough minimum location (Foster et al., 2007).

It has been well known that the location of the midlatitude trough moves equatorward during high geomagnetic activity conditions (e.g., Krankowski et al., 2009; Yang et al., 2015). Yizengaw et al. (2005) showed a good correlation between the midlatitude trough and the plasmapause for geomagnetically quiet and disturbed conditions using the IMAGE EUV map and global ionospheric maps (GIM) of total electron content (TEC). However, they did not perform a detailed investigation of the characteristics of temporal and spatial variations of the midlatitude trough due to the limitation of using GIM of TEC. Combining GPS TEC and the Poker Flat incoherent scatter radar and all-sky imagers, Zou et al. (2011) investigate the dynamics of the midlatitude trough during several nonstorm time substorm events for solar minimum conditions in the Alaska region. They found that the poleward density gradient shifts equatorward rapidly after substorm onset with a maximum speed of 4–5° of geomagnetic latitude per hour. The equatorward-shifted trough disappeared due to enhanced energetic electron precipitation associated with the development of substorms. After the start of the recovery phase, the midlatitude trough tended to reappear. However, since their study focuses on the dynamics of the midlatitude trough during the nonstorm time substorm events in the Alaska region, the temporal variation of the longitudinal distribution of the storm time midlatitude trough remains unknown. Therefore, none of these recent researches have shown a large-scale (>1,000 km) structure of the midlatitude trough in the longitudinal direction and its temporal variation associated with a geomagnetic storm.

In this paper, we investigate the temporal and spatial variations of the midlatitude trough in the ionosphere with high resolution during a geomagnetic storm which occurred on 4 April 2017, based on an integrated data analysis of ground dense Global Navigation Satellite System (GNSS) receiver network and satellite observations. In particular, we report the characteristics of geomagnetic latitude and longitude variations of the trough minimum location with high time and spatial resolutions during a geomagnetic storm.

2. Observation Data and Analysis Method

2.1. Observation Data Set

We use the absolute GNSS-TEC data with time resolution of 30 s obtained from many dense regional and worldwide international GNSS receiver networks. A detailed method to derive the absolute GNSS-TEC data was found by Otsuka et al. (2002). The GNSS-TEC data have been stored in the dense regional and worldwide international GNSS-TEC observation (DRAWING-TEC) database managed by the National Institute of Information and Communications Technology in Japan (http://seg-web.nict.go.jp/GPS/DRAWING-TEC/). The GNSS-TEC data are derived from the GNSS data obtained from a large number of GNSS stations (more than 10,000 in September 2017). Detailed information of this GNSS-TEC database and its derivation method are described by Tsugawa et al. (2007, 2018). In this analysis, we perform the 5-min average of the available grid GNSS-TEC data having a spatial resolution of $0.5 \times 0.5°$ in geographical latitude and longitude. The grid data are averaged every 0.5° with the data included in four bins (0.25×0.25 °).

The Arase satellite was launched at 11:00 (UT) on 20 December 2016 from Uchinoura Space Center. The satellite has been put into a geo-transfer orbit with an inclination of 31°, with initial apogee and perigee of 32,110 and 460 km, respectively. The orbital period is 565 min (Miyoshi, Shinohara, et al., 2018). In the present study, we analyze plasma wave dynamic spectrum data provided by High-Frequency Analyzer (HFA; Kumamoto et al., 2018), which is a subcomponent of the Plasma Wave Experiment (PWE; Kasahara et al., 2018) onboard the Arase satellite to identify the upper limit frequency of upper hybrid resonance waves along the satellite

orbit. In this study, we use the electric field spectrum data of plasma waves with time resolution of 1 or 8 s. The Common Data Format data of the HFA plasma wave spectrum are provided by ERG Science Center, Nagoya University (https://ergsc.isee.nagoya-u.ac.jp/data_info/index.shtml.en; Miyoshi, Hori, et al., 2018).

In order to investigate solar wind, IMF, and geomagnetic activity conditions during a geomagnetic storm which occurred on 4 April 2017, we use the high-resolution OMNI data provided by Coordinated Data Analysis Web (CDAWeb); NASA (https://cdaweb.sci.gsfc.nasa.gov/index.html); geomagnetic indices (*AE* and *SYM-H*) provided by World Data Center for Geomagnetism, Kyoto University (http://wdc.kugi.kyoto-u.ac.jp); and geomagnetic field data at the Pinawa station (PINA; 59.98 and 331.75° in geomagnetic latitude and longitude), belonging to the Carisma site (http://www.carisma.ca). We also use a list of geomagnetically quiet and disturbed days provided by World Data Center for Geomagnetism, Kyoto University to produce the average GNSS-TEC grid data of 10 geomagnetically quiet days in April 2017. We further use the common time Super Dual Auroral Radar Network (SuperDARN) radar data in Common Data Format (Hori et al., 2013) in North America and Japan provided by ERG Science Center, Nagoya University (https://ergsc.isee.nagoya-u.ac.jp/data_info/index.shtml.en).

### 2.2. Global GNSS TEC Data Analysis Method

Because the electron density profile of the ionosphere depends strongly on local time, geographical latitude, and longitude, the absolute GNSS-TEC data also show a similar dependence to the ionospheric electron density profile. Therefore, to identify the storm time fluctuation component of the GNSS-TEC data, we subtract the background component from the storm time GNSS-TEC data in April 2017. As a first step, to obtain the background GNSS-TEC data, we refer to a list of geomagnetically quiet and disturbed days and calculate the average GNSS-TEC grid data of 10 geomagnetically quiet days in April 2017. As a next step, we subtract the average GNSS-TEC grid data from the storm time GNSS-TEC data every 5 min. The subtracted data are plotted as a two-dimensional map in geographical or geomagnetic coordinates as shown in Figures 1g, 1h, and 2a, respectively. In converting the GNSS-TEC data into the geomagnetic coordinates, we use the Altitude Adjusted Corrected GeoMagnetic model (Shepherd, 2014). For identification of the trough minimum location from the subtracted GNSS-TEC data, we perform a pixel smoothing with a boxcar window of $1.5 \times 1.5°$ in geographic latitude and longitude. This procedure determines the average TEC value at the center of the window using nine grids since the spatial resolution of the raw data is $0.5 \times 0.5°$. And, the boxcar window is shifted by 0.5° in the latitude and longitude directions. Therefore, since this procedure smooths the data in a range of $1.5 \times 1.5°$, we can investigate the spatial variation of the trough minimum location with a scale of more than 150 km. Furthermore, we perform the 30-min running average for the GNSS-TEC keograms at each longitude obtained from the pixel smoothing data. Finally, we determine the minimum value of GNSS-TEC in each keogram as the trough minimum.
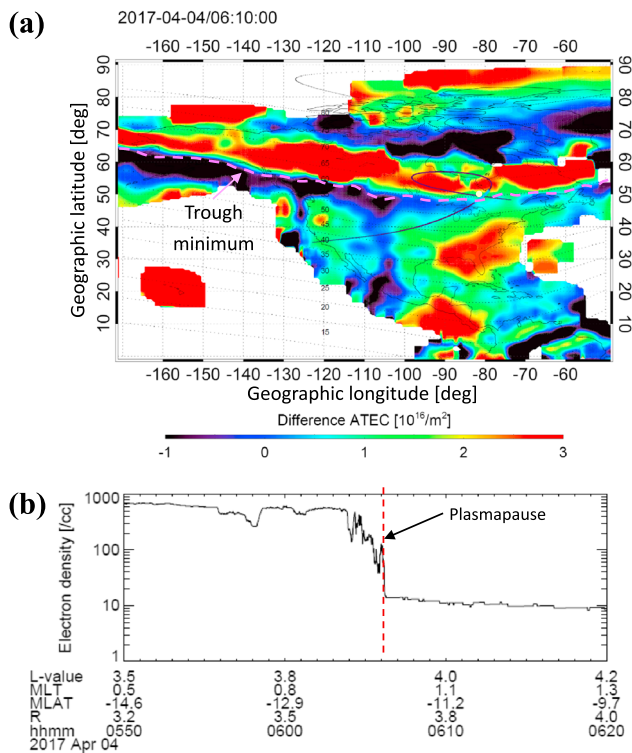
3. Results and Discussion

3.1. Overview of a Geomagnetic Storm Event on 4 April 2017

Figure 1 shows an overview of the geomagnetic storm event which occurred on 4 April 2017, and GNSS-TEC polar maps in the northern hemisphere plotted with the Altitude Adjusted Corrected GeoMagnetic coordinates at 04:00, 06:00, and 08:00 (UT) corresponding to the prestorm, main, and maximum phases. In the Figures 1a–1f, the geomagnetic storm commences at 04:40 (UT) as a sudden increase of *SYM-H* associated with the arrival of a solar wind dynamic pressure enhancement. After that, the B_z component of IMF is directed southward with a significant magnitude of ~10 nT, and the *SYM-H* index shows an abrupt decrease of ~50 nT within 2 hr. Associated with northward turning of IMF B_z at 11:00 (UT), the recovery phase starts as an increasing *SYM-H* value.

The GNSS-TEC polar map at the prestorm phase (Figure 1g) shows a complex spatial TEC variation as a function of geomagnetic latitude and longitude. The most remarkable feature of the TEC variation is an enhancement of TEC in the duskside (12–23 h magnetic local time (MLT)) along the geomagnetic latitude of ~70° in geomagnetic latitude (GMLAT). At a lower latitude, the midlatitude trough can be clearly seen as a narrow-decreased TEC region between 18 and 01 h (MLT). During the main phase, the GNSS-TEC polar map (Figure 1h) shows that the enhanced TEC region at 60–65° (GMLAT) extends to the postmidnight sector (~3 h, MLT), and that the midlatitude trough also appears at a lower latitude (55–60°, GMLAT) of the
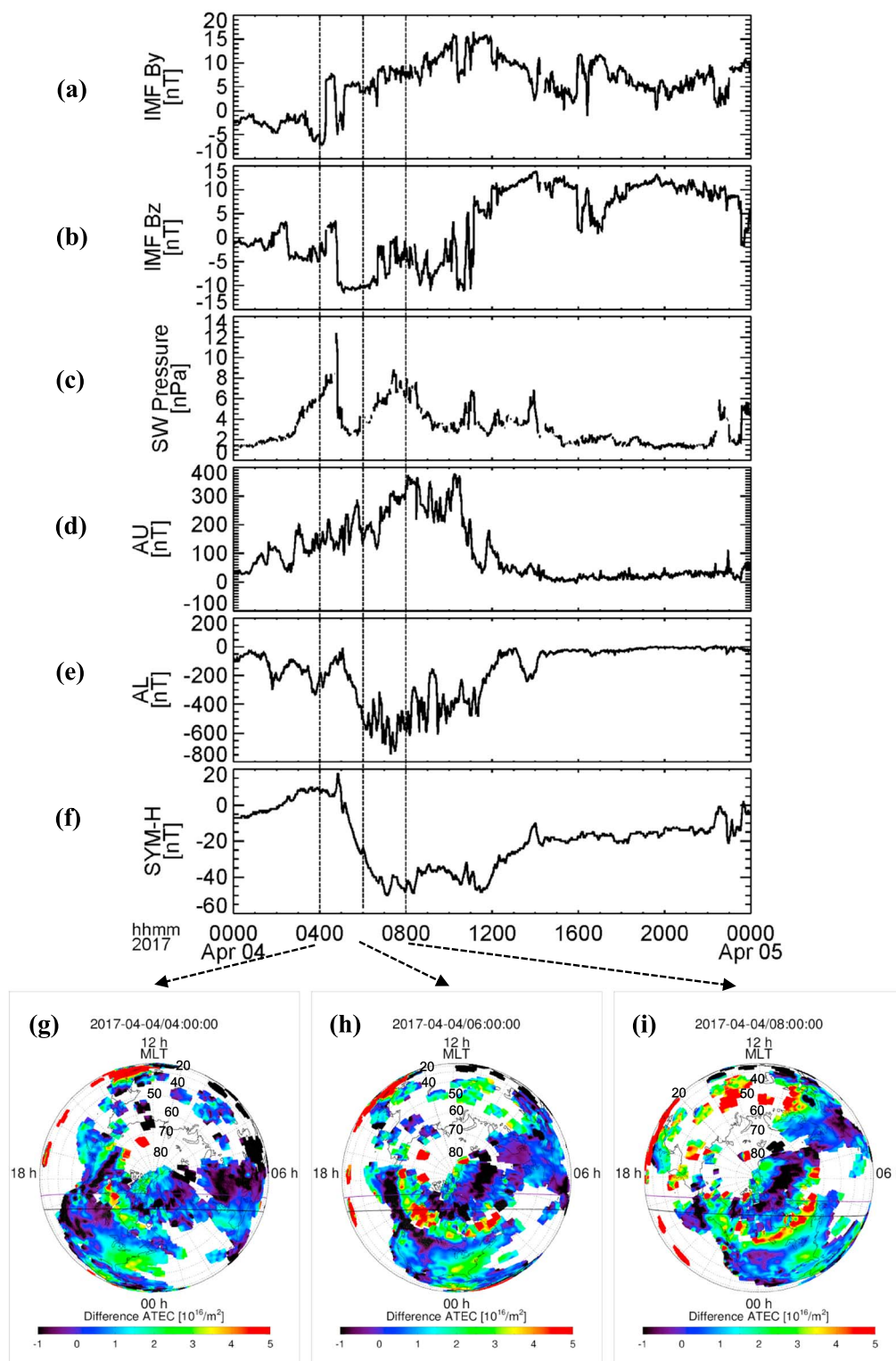
Figure 1. (a–f) Time series plot of high-resolution OMNI data (IMF by B_z, solar wind dynamic pressure, and geomagnetic indices (AU, AL, and SYM-H)) within a time interval from 00:00 (UT) on 4 April to 00:00 (UT) on 5 April 2017 and (g–i) global GNSS-TEC polar maps in AACGM coordinates at 04:00, 06:00, and 08:00 (UT) corresponding to the prestorm, main, and maximum phases of the geomagnetic storm, respectively. The vertical dashed lines show the time of each global GNSS-TEC map. The color code of each GNSS-TEC map indicates a difference value of absolute TEC (ATEC) from the average TEC of 10 geomagnetically quiet days. The black and purple curves represent the day-night terminator at 300 and 110 km, respectively. The number from 20 to 80 in (g)–(i) shows the geomagnetic latitude.

AGU
100
ADVANCING EARTH
AND SPACE SCIENCE

Geophysical Research Letters

10.1029/2018GL078723

(a)

2017-04-04/06:10:00

(b)

Figure 2. (a) Two-dimensional GNSS-TEC map in North America in geographical coordinates at 06:10 (UT) on 4 April 2017 and (b) electron density along the Arase satellite orbit from 05:50 to 06:10 (UT). The black curve in the GNSS-TEC map shows the footprint of the Arase satellite orbit at an ionospheric height of 100 km from 05:00 to 13:40 (UT). The light blue part of this curve corresponds to the Arase orbit shown in (b). The solid circle with a yellow color on the Arase orbit curve shows the location of the plasmapause. The dashed pink curve is the location of the midlatitude trough minimum. The orbit information of the Arase satellite is shown in the bottom of (b). The vertical dashed line in (b) indicates the location of the plasmapause identified from the electron density profile.

enhanced TEC region between 17 and 3 h (MLT). The GNSS-TEC polar map (Figure 1i) during the maximum phase of the geomagnetic storm also shows an extension of the enhanced TEC region up to the dawnside (~6 h, MLT) and the dayside TEC enhancement in the middle- and low-latitude regions (8–18 h, MLT). The TEC enhancement in the auroral zone can be considered to be attributed to an enhancement of auroral precipitation which leads to an increase in the ionization rate in the ionosphere (e.g., Lu et al., 1998). On the other hand, the dayside TEC enhancement in the midlatitude trough is considered as a part of the SED generated by local imbalance of the plasma loss and production processes (e.g., Heelis et al., 2009; Huba & Sazykin, 2014; Lu et al., 2012; Zou et al., 2013, 2014).

3.2. Comparison Between the GNSS-TEC and Arase Observations in North America

Figure 2 shows a two-dimensional GNSS-TEC map in North America in geographical coordinates at 06:10 (UT) on 4 April 2017 and electron density derived from the upper limit frequency of the upper hybrid resonance waves in a time interval between 05:50 and 06:10 (UT). In calculating the electron density along the Arase satellite orbit, we use 8-s spin-averaged total magnetic field intensity data obtained from the Magnetic Field Experiment (MGF) instrument (Matsuoka et al., 2018) onboard the Arase satellite. The GNSS-TEC map (Figure 2a) shows an enhanced TEC region with a belt-shaped structure along the geomagnetic longitude. At the lower latitude edge of the enhanced TEC region, the midlatitude trough appears as a decreased TEC region. The electron density profile in the inner magnetosphere (Figure 2b) shows an abrupt drop with an irregular variation from 497 to 13.8 [/cc] within an L value of 0.2 in the postmidnight (~1 h, MLT). The electron density drop indicates the plasmapause signature as defined by Carpenter and Anderson (1992), and the footprint of the plasmapause (indicated by a dashed line in the Figure 2b) at an ionospheric altitude of 300 km is approximately 59° (GMLAT). The location is close to the location (58°, GMLAT) of the trough minimum. This good agreement between both locations is consistent with the results of Yizengaw et al. (2005), who showed that the trough minimum location corresponds to the nighttime plasmapause (22–04 h, MLT). From this result, we confirm that the nighttime trough minimum derived from the present GNSS-TEC data analysis can be used to monitor the temporal and spatial variations of the plasmapause.

3.3. Characteristics of Geomagnetic Latitudinal and Longitudinal Variations of the Trough Minimum Location in North America

To investigate the characteristics of geomagnetic latitudinal and longitudinal variations of the storm time trough minimum location, we create a GNSS-TEC keogram in the three geomagnetic longitudes in North America. Because several dense GNSS receiver networks have been extended to a wide range of geomagnetic latitude and longitude in North America, this region is suitable for investigation of temporal and spatial variations of the trough minimum location. Figure 3 shows the time series plot of the *SYM-H* index and H component (north-south) of the geomagnetic field at the PINA station and keogram of the GNSS-TEC data in three different geomagnetic longitudes in a time interval between 02:00 and 20:00 (UT) on April 2017. The white line in Figures 3c–3f indicates the trough minimum locations that are identified from the minimum value of TEC in a latitudinal width of ±5°. The window center at each time is determined by the trough minimum location just before the time. In this case, the initial latitude of the window center is 60° at 02:00 (UT). In this figure, the trough minimum location indicated by the white line moves equatorward in all geomagnetic longitude sectors as the geomagnetic storm develops. The movement speed clearly increases from 1.3 to 3.5° of geomagnetic latitude per hour in two sectors (325.75 and 350.82°, GMLONG) after the onset of the geomagnetic field variations at PINA associated with the substorm. The enhancement of the movement speed
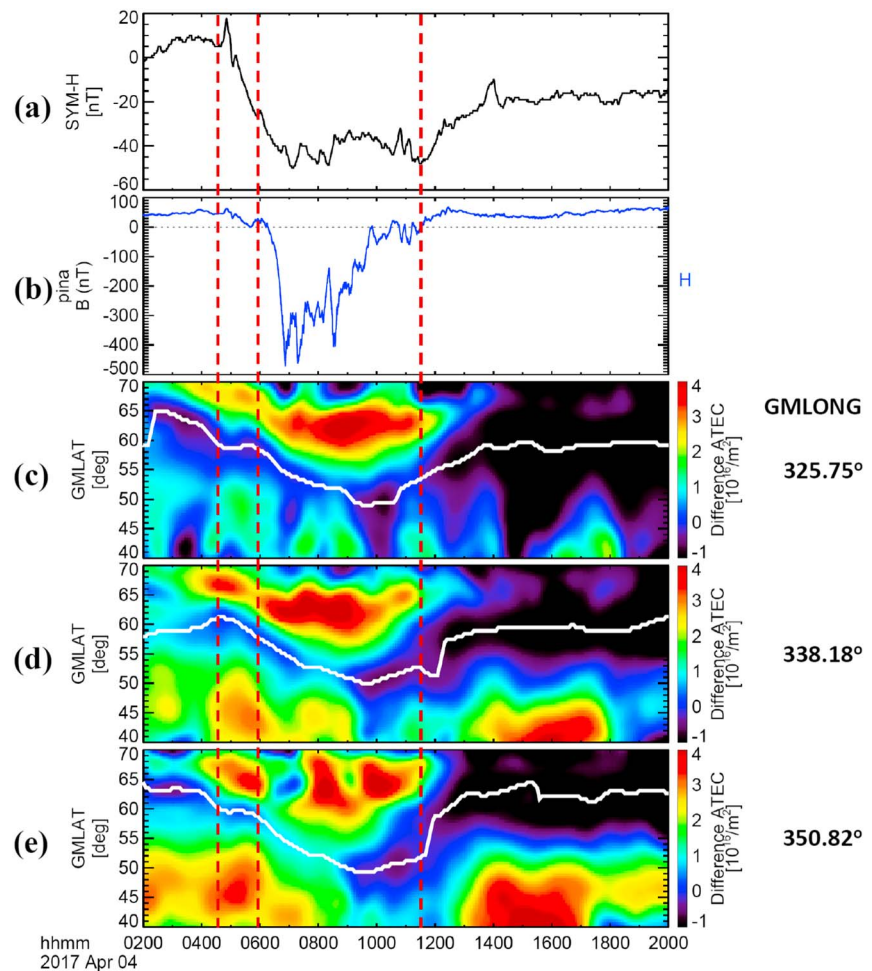
Figure 3. Time series plot of the (a) *SYM-H* index and (b) *H* component of the geomagnetic field at the PINA station and (c) keogram of the GNSS-TEC data in three different geomagnetic longitudes in a time interval between 02:00 and 20:00 (UT) on April 2017. The right label H in (b) indicates the north-south component of the geomagnetic field in geographic coordinates, respectively. The color bars in (c)–(e) indicate a difference value of absolute TEC in a range of −1–4 TEC unit. The white line in each keogram shows the location of the midlatitude trough minimum identified from the minimum value of GNSS-TEC. The three vertical dashed lines represent the geomagnetic storm commencement and the onsets of substorm and storm recovery phase, respectively.

means a rapid shrinking of the plasmasphere due to the enhanced electric field associated with substorm. After the start of the recovery phase of the substorm or geomagnetic storm, the trough minimum location rapidly moves poleward back to the quiet time location within 4 hr. The average speed of the poleward movement is 2.3° of geomagnetic latitude per hour. This behavior is basically consistent with the result reported by Zou et al. (2011), but the present study also showed a variation of geomagnetic longitudinal response of the trough minimum.

Figure 4 shows the time series plot of the *AE* and *SYM-H* indices and contour plot of the trough minimum location between 300 and 360° (GMLONG; Figures 4a–4c) and the cross sections of the contour plot at 08:30, 10:00, and 11:30 (UT; Figures 4d–4f), respectively. In these panels, we overplot the trough minimum locations as a blue triangle determined from the raw GNSS-TEC grid data (0.5 × 0.5°) to verify that the significant variation is not induced by the spatial smoothing procedure. For comparison of the trough minimum location between the storm and quiet times, we add the trough minimum location at the same UT during a quiet time (16 April 2017) as a purple line in Figures 4d–4f. In these panels, a significant longitudinal variation of the trough minimum location is clearly found during both the storm and quiet times, although the pattern of the longitudinal variation is different between both the periods. The scale is 10–25° (GMLONG;
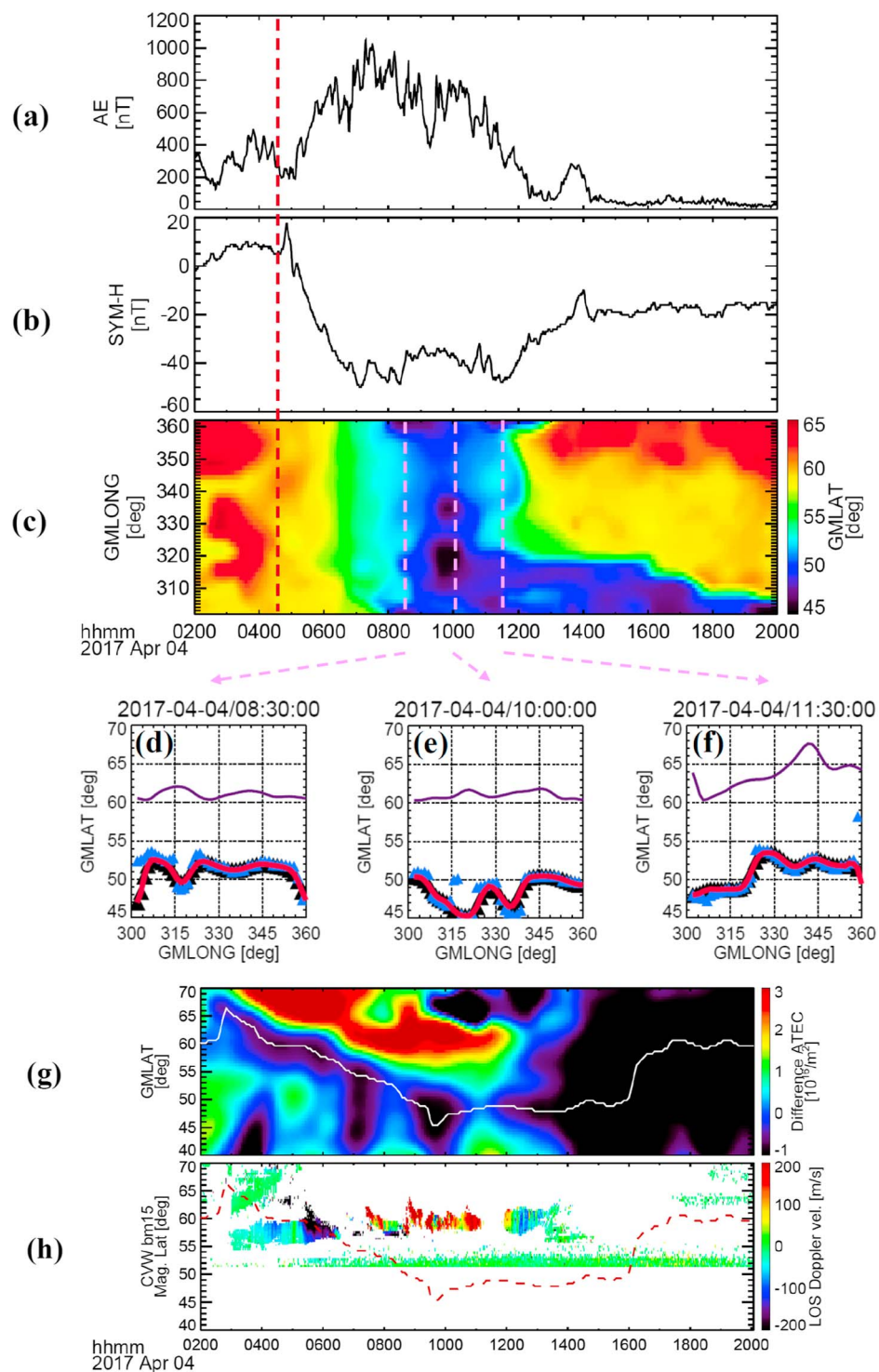
Figure 4. (a–c) Time series plot of the *AE* and *SYM-H* indices and contour plot of the trough minimum location as a function of time and geomagnetic longitude; (d–f) the cross sections in (c) at 08:30, 10:00, and 11:30 (UT); and the (g and h) GNSS-TEC keogram and ionospheric plasma flow in the beam-15 direction observed with the SuperDARN radar at Christmas Valley west. The color bars in (c), (g), and (h) show the geomagnetic latitude of the trough minimum location, the difference TEC value, and Doppler velocity in the beam-15 direction. The red dashed line in (a)–(c) indicates the storm commencement, and the three dashed pink lines in (c) represents the time of the three bottom panels. The blue and black triangles (or red line) in panels (d) and (e) show the trough minimum location determined by the raw and smoothing data. The purple line indicates the trough minimum location during a geomagnetically quiet day on 16 April 2017. The white and red dashed lines in (g) and (h) represent the trough minimum location.

1,000–2,500 km). Moreover, as shown in Figure 4c, the storm time trough minimum location moves equatorward and back to the quiet time location during the main and recovery phases, respectively. It is noted that the longitudinal distribution of the trough minimum in a region of 320–360° (GMLONG) does not show a remarkable change after 13:00 (UT) during the recovery phase.

Although most of the previous studies have shown that the location of the midlatitude trough depends on season, local time, and the response to the geomagnetic conditions by a case and statistical analysis of the GPS TEC data (e.g., Krankowski et al., 2009; Zou et al., 2011), we have found that the longitudinal distribution indicates a significant variation of the trough minimum location with a scale of 1,000–2,500 km. Although Yizengaw et al. (2005) analyzed the local time variation of the trough minimum location from GIM of TEC, they did not show the local time distribution of the trough minimum and its temporal variation with high resolution due to limitations of GIM of TEC. From the present (Figure 2) and previous (Yizengaw et al., 2005) analysis results, it can be considered that the significant variation of the trough minimum reflects a structure in the shape of the plasmasphere in the MLT direction. Considering the origin of the midlatitude trough as described in Schunk et al. (1976), the longitudinal variation of the trough minimum might be related to the longitudinal distribution of the SAPS electric field. To prove or disprove this hypothesis, we compare the GNSS-TEC keogram with ionospheric plasma flow in the beam-15 direction observed with the SuperDARN radar at Christmas Valley West (Figures 4g and 4h). The westward plasma flow identified as the SAPS phenomena appears in the auroral zone (62–65°, GMLAT) after the onset of the geomagnetic storm. After 05:20 (UT), the westward plasma flow expands to the midlatitude region, almost coinciding with the restart of the equatorward movement of the trough minimum. This result suggests that the westward flow is related to the formation of the midlatitude trough. However, the trough minimum is located at a lower latitude than the observation region of the SuperDARN radar for a period (08:00–12:00 (UT)) when the significant variation of the trough minimum is observed. This situation does not change for the other midlatitude SuperDARN radars in North America as shown in supporting information S1–S4. Therefore, we could not prove the hypothesis that the longitudinal variation of the trough minimum is caused by a spatial distribution of the SAPS electric field in the present data analysis. This point should be investigated in future studies.

4. Conclusions

To clarify the characteristics of temporal and spatial variations of the trough minimum location during a geomagnetic storm which occurred on 4 April 2017, we analyze the 5-min average GNSS-TEC data together with solar wind, IMF, geomagnetic field, and Arase PWE-HFA observation data. Our analysis reveals the following results:

1. After the onset of the geomagnetic storm, the trough minimum location moves equatorward from 60 to 48° within 4 hr. The equatorward movement implies a shrinking of the plasmasphere due to an enhanced convection electric field in the inner magnetosphere associated with the geomagnetic storm.
2. The trough minimum location identified from the minimum value of the GNSS-TEC data from the auroral to midlatitude regions is in good agreement with that of the plasmapause observed by the Arase satellite with a difference of geomagnetic latitude by 1–2°.
3. The longitudinal variation of the trough minimum location shows a significant variation with its scale of 1,000–2,500 km during both the storm and quiet times. This phenomenon has not yet been reported by previous studies due to limitations in the coverage density of GNSS receiver networks.
4. After the start of the recovery phase, the trough minimum location rapidly moves poleward back to the quiet time location within 4 hr in a geomagnetic longitude range of 310–360° in geomagnetic longitude.

References

Carpenter, D. L., & Anderson, R. R. (1992). An ISEE/whistler model o equatorial electron density in the magnetosphere. *Journal of Geophysical Research*, 97, 1097–1108. https://doi.org/10.1029/91JA01548

Foster, J. C. (1993). Storm time plasma transport at middle and high latitudes. *Journal of Geophysical Research*, 98, 1675–1689. https://doi.org/10.1029/92JA02032

Foster, J. C., Coter, A. J., Erickson, P. J., Rich, F. J., & Sandel, B. R. (2004). Stormtime observations of the flux of plasmaspheric ions to the dayside cusp/magnetopause. *Geophysical Research Letters*, 31, L08809. https://doi.org/10.1029/2004GL020082

Foster, J. C., Erickson, P. J., Coster, A. J., Goldstein, J., & Rich, F. J. (2002). Ionospheric signatures of plasmaspheric tails. *Geophysical Research Letters*, 29(13), 1623. https://doi.org/10.1029/2002GL015067

Foster, J. C., & Rideout, W. (2005). Midlatitude TEC enhancements during the October 23 superstorm. *Geophysical Research Letters*, *32*, L12S04. https://doi.org/10.1029/2004GL021719

Foster, J. C., Rideout, W., Sandel, B., Forrester, W. T., & Rich, F. J. (2007). On the relationship of SAPS to storm enhanced density. *Journal of Atmospheric Space Terrestrial Physics*, *69*(3), 303–313. https://doi.org/10.1016/j.jastp.2006.07.021

Foster, J. C., & Vo, H. B. (2002). Average characteristics and activity dependence of the subauroral polarization stream. *Journal of Geophysical Research*, *107*(A12), 1475. https://doi.org/10.1029/2002JA009409

Goldstein, J., & Sandel, B. R. (2005). The global pattern of evolution of plasmaspheric drainage plumes, *Inner Magnetosphere Interactions: New Perspectives From Imaging*. *Geophysical. Monograph Series*, *159*, 1.

Heelis, R. A., Sojka, J. J., David, M., & Schunk, R. W. (2009). Storm time density enhancements in the middle-latitude dayside ionosphere. *Journal of Geophysical Research*, *114*, A03315. https://doi.org/10.1029/2008JA013690

Hori, T., Nishitani, N., Miyoshi, Y., Miyashita, Y., Seki, K., Segawa, T., et al. (2013). An integrated analysis platform merging the SuperDARN data within the THEMIS tool developed by ERG-Science Center (ERG-SC). *Advances in Polar Science*, *24*, 69–77. https://doi.org/10.3724/SP.J.1085.2013.000692013

Huba, J. D., & Sazykin, S. (2014). Storm time ionosphere and plasmasphere structuring: SAMI3-RCM simulation of the 31 March 2001 geomagnetic storm. *Geophysical Research Letters*, *41*, 8208–8214. https://doi.org/10.1002/2014GL062110

Kasahara, Y., Kasaba, Y., Kojima, H., Yagitani, S., Ishisaka, K., Kumamoto, A., et al. (2018). The plasma wave experiment (PWE) on board the Arase (ERG) satellite. *Earth, Planets and Space*, *70*(1), 86. https://doi.org/10.1186/s40623-018-0842-4

Krankowski, A., Shagimuratov, I. I., Ephishov, I. I., Krypiak-Gregorczyk, A., & Yakimova, G. (2009). The occurrence of the mid-latitude ionospheric trough in GPS-TEC measurements. *Advances in Space Research*, *43*(11), 1721–1731. https://doi.org/10.1016/j.sar.2008.05.014

Kumamoto, A., Tsuchiya, F., Kasahara, Y., Kasaba, Y., Kojima, H., Yagitani, S., et al. (2018). High frequency analyzer (HFA) of plasma wave experiment (PWE) onboard the Arase spacecraft. *Earth, Planets and Space*, *70*(1), 82. https://doi.org/10.1186/s40623-018-0854-0

Lu, G., Goncharenko, L., Nicolls, M. J., Maute, A., Coster, A., & Paxton, L. J. (2012). Ionospheric and thermospheric variations associated with prompt penetration electric fields. *Journal of Geophysical Research*, *117*, A08312. https://doi.org/10.1029/2012JA017769

Lu, G., Pi, X., Richmond, A. D., & Roble, R. G. (1998). Variations of total electron content during geomagnetic disturbances: A model/observation comparison. *Geophysical Research Letters*, *25*, 253–256. https://doi.org/10.1029/97GL03778

Matsuoka, A., Teramoto, M., Nomura, R., Nosé, M., Fujimoto, A., Tanaka, Y., et al. (2018). The ARASE (ERG) magnetic field investigation. *Earth, Planets and Space*, *70*, 43. https://doi.org/10.1186/s40623-018-0800-1

Miyoshi, Y., Hori, T., Shoji, M., Teramoto, M., Chang, T. F., Segawa, T., et al. (2018). The ERG science center. *Earth, Planets and Space*, *70*(1), 96. https://doi.org/10.1186/s40623-018-0867-8

Miyoshi, Y., Shinohara, I., Takashima, T., Asamura, K., Higashio, N., Mitani, T., et al. (2018). Geospace Exploration Project ERG. *Earth, Planets and Space*, *70*(1). https://doi.org/10.1186/s40623-018-0862-0

Moldwin, M. B., Howard, J., Sanny, J., Bocchicchio, J. D., Rassoul, H. K., & Anderson, R. R. (2004). Plasmaspheric plumes: CRRES observations of enhanced density beyond the plasmapause. *Journal of Geophysical Research*, *109*, A05202. https://doi.org/10.1029/2003JA010320

Otsuka, Y., Ogawa, T., Saito, A., Tsugawa, T., Fukao, S., & Miyazaki, S. (2002). A new technique for mapping of total electron content using GPS network in Japan. *Earth, Planets and Space*, *54*(1), 63–70. https://doi.org/10.1186/BF03352422

Schunk, R. W., Banks, P. M., & Raitt, W. J. (1976). Effects of electric fields and other processes upon the nighttime high-latitude F layer. *Journal of Geophysical Research*, *81*, 3271–3282. https://doi.org/10.1029/JA081i019p03271

Shepherd, S. G. (2014). Altitude-adjusted corrected geomagnetic coordinates: Definition and functional approximations. *Journal of Geophysical Research: Space Physics*, *119*, 7501–7521. https://doi.org/10.1002/2014JA020264

Tsugawa, T., Kotake, N., Otsuka, Y., & Saito, A. (2007). Medium-scale traveling ionospheric disturbances observed by GPS receiver network in Japan: A short review. *GPS Solutions*, *11*(2), 139–144. https://doi.org/10.1007/s10291-006-0045-5

Tsugawa, T., Nishioka, M., Ishii, M., Hozumi, K., Saito, S., Shinbori, A., et al. (2018). Total electron content observations by dense regional and worldwide international networks of GNSS. *Journal of Disaster Research*, *13*(3), 535–545. https://doi.org/10.20965/jdr.2018.p0535

Tsurutani, B. T., Gonzalez, W. D., Gonzalez, A. L. C., Guarnieri, F. L., Gopalswamy, N., Grande, M., et al. (2006). Corotating solar wind streams and recurrent geomagnetic activity: A review. *Journal of Geophysical Research*, *111*, A07S01. https://doi.org/10.1029/2005JA011273

Yang, N., Le, H., & Liu, L. (2015). Statistical analysis of ionospheric mid-latitude trough over the northern hemisphere derived from GPS total electron content data. *Earth, Planets and Space*, *67*(1), 196. https://doi.org/10.1186/s40623-015-0365-1

Yizengaw, E., Dewar, J., MacNeil, J., Moldwin, M. B., Galvan, D., Sanny, J., et al. (2008). The occurrence of ionospheric signatures o plasmaspheric plumes over different longitudinal sectors. *Journal of Geophysical Research*, *113*, A08318. https://doi.org/10.1029/2007JA012925

Yizengaw, E., Moldwin, M. B., & Galvan, D. A. (2006). Ionospheric signatures of a plasmaspheric plume over Europe. *Geophysical Research Letters*, *33*, L17103. https://doi.org/10.1029/2006/GL026597

Yizengaw, E., Wei, H., Moldwin, M. B., Galvan, D., Mandrake, L., Mannucci, A., & Pi, X. (2005). The correlation between mid-latitude trough and the plasmapause. *Geophysical Research Letters*, *32*, L10102. https://doi.org/10.1029/2005/GL022954

Zou, S., Moldwin, M. B., Coster, A., Lyons, L. R., & Nicolls, M. J. (2011). GPS TEC observations of dynamics of the mid-latitude trough during substorms. *Geophysical Research Letters*, *38*, L14109. https://doi.org/10.1029/2011GL048178

Zou, S., Moldwin, M. B., Ridley, A. J., Nicolls, M. J., Coster, A. J., Thomas, E. G., & Ruohoniemi, J. M. (2014). On the generation/decay of the storm-enhanced density plumes: Role of the convection flow and field-aligned ion flow: Generation and decay of SED plumes. *Journal of Geophysical Research: Space Physics*, *119*, 8543–8559. https://doi.org/10.1002/2014JA020408

Zou, S., Ridley, A. J., Moldwin, M. B., Nicolls, M. J., Coster, A. J., Thomas, E. G., & Ruohoniemi, J. M. (2013). Multi-instrument observations of SED during 24–25 October 2011 storm: Implications for SED formation processes. *Journal of Geophysical Research: Space Physics*, *118*, 7798–7809. https://doi.org/10.1002/2013JA018860